Oceland: A conceptual model for ocean-land-atmosphere interactions based on water balance equations

Luca Schmidt[a] , Cathy Hohenegger[a]

[a] *Max Planck Institute for Meteorology, Hamburg*

Corresponding author: Luca Schmidt, luca.schmidt@mpimet.mpg.de

ABSTRACT: What processes control the partitioning of precipitation between land and ocean? Do large-scale constraints exist? We address these questions using a conceptual box model based on water balance equations. With empirical but physically motivated parametrizations of the water balance components, we construct a set of coupled differential equations which describes the dynamical behavior of the water vapor content over land and ocean as well as the land's soil moisture content. For a closed model configuration with one ocean and one land box, we compute equilibrium solutions across the parameter space and analyze their sensitivity to parameter choices. The precipitation ratio χ, defined as the ratio between mean land and ocean precipitation rates, quantifies the precipitation partitioning. We find that χ is confined to a range between zero and one and that it is primarily controlled by the efficiency of atmospheric moisture transport and, to a lesser extent, by surface characteristics. Precipitation enhancement over land, $\chi > 1$, is only possible by relaxing the model assumptions. An open model configuration with an island between two ocean boxes and nonzero external advection into the domain yields stronger land precipitation for a small subset of parameter choices, characterized by small land fractions and a sufficiently large moisture influx through the windward boundary. All in all, we conclude that especially small-scale systems cannot be adequately described without a diurnal cycle and that the land is likely to affect the relationship between water vapor path and precipitation.

1. Introduction

All water that evaporates from Earth's land and ocean surfaces must eventually return to the surface as precipitation. But which physical processes or parameters of the system determine how precipitation gets partitioned between land and ocean? Ought land or ocean receive more rain on average? And do large-scale constraints on the partitioning exist based on fundamental water balance equations? Modern observations provide comprehensive descriptions of real-world precipitation partitioning but typically do not reveal the underlying reasons. Similarly, the complexity of sophisticated climate models limits clear process understanding and, apart from that, these models frequently fail to reproduce observed precipitation patterns (Fiedler et al. (2020)). It is therefore the aim of this study to explain precipitation partitioning with a simple box model describing a coupled land-ocean-atmosphere system.

In a recent study, Hohenegger and Stevens (2022) computed the ratio of spatially averaged precipitation rates over tropical land and ocean, χ, from different observational datasets and found values between $\chi = 0.9$ and 1.04. These values, reflecting nearly equal mean rain rates over land and ocean, are somewhat surprising given that the two surface types have very different characteristics and interact with the atmosphere in different ways. Most notably, the land can dry out and thereby significantly reduce the moisture input into the atmosphere through evapotranspiration while ocean evaporation is never moisture-limited.

The interaction between soil moisture and precipitation has been widely studied with the help of conceptual models. In a seminal paper, Budyko and Drozdov (1953) introduced a one-dimensional land-atmosphere model in which a horizontal airstream traverses a continental region. Starting from a given moisture content at the windward boundary the airstream moistens or dries along the passage depending on the relative magnitude of the region's mean precipitation and surface evapotranspiration. Since this framework distinguishes between precipitation from advected moisture from outside and locally evaporated moisture from within the region, it formed the basis for several moisture recycling studies which assessed the importance of locally evaporated moisture for precipitation in the same region (see Burde and Zangvil (2001) for a review of adaptations of the Budyko model and its general limitations).

Brubaker et al. (1993) and Eltahir and Bras (1994) are two examples which extended the Budyko model to two dimensions and used observations to quantify the water balance components. They

found varying but moderate contributions from local moisture to precipitation for a number of innercontinental regions. Using a global accounting technique, Ent et al. (2010) demonstrated that reevaporated moisture from continental surfaces is indeed important for land precipitation in many parts of the world and sometimes even the predominant contribution. For the question of precipitation partitioning, however, the origin of precipitated moisture is secondary. What matters is the amount of moisture that the land receives from the ocean in the first place and how much of this moisture is turned into precipitation in subsequent recycling loops before the moist air mass leaves the land again. This is best assessed through statistical analyses.

Bretherton et al. (2004) were the first to establish a statistical relationship between spatio-temporal mean precipitation rate P and water vapor pass w over tropical oceans. Based on observations, they found an exponential relationship between the atmospheric moisture content and precipitation, $P(w)$, in which precipitation increases strongly beyond some pick-up value of w. Similar results were obtained by Schiro et al. (2016) and Schiro et al. (2020) for the Amazon, suggesting that the processes which turn moisture into precipitation are not significantly affected by the underlying surface type. However, Ahmed and Schumacher (2017) compared the $P(w)$-relationship over land and ocean regions across the tropics and for different times of the day and found lower pick-up values for land regions. They also showed that pick-up values over land get shifted during the course of a day, presumably due to stronger surface heating compared to the ocean and orographic effects. Bergemann and Jakob (2016) added that the relationship between tropical *coastal* precipitation and water vapor pass differs from both the open ocean and inland areas but they also found an exponential shape in all cases.

The fact that moisture fluxes are found to be directly related to available moisture suggests the usage of box models which treat the land and atmosphere as well-mixed moisture reservoirs. Moisture balance equations which describe the change of soil moisture and atmospheric water content as the sum of moisture sinks and sources were formulated, for instance, by Horton (1943) and Peixóto and Oort (1983). Rodriguez-Iturbe et al. (1991) and Entekhabi et al. (1992), studying the stochastical-dynamical behaviour of continental hydrology, utilized the soil moisture balance equation in equilibrium to express the moisture fluxes in the Budyko framework as functions of relative soil moisture saturation. Brubaker and Entekhabi (1995) developed a box model of continental land-atmosphere interactions consisting of coupled water and energy balance equations

for soil and atmosphere reservoirs of both moisture and heat. They used this conceptual model to study the system's equilibrium behavior and in a follow-up publication the role of land-atmosphere feedbacks in the response to stochastic perturbations of horizontal wind speed and solar irradiation (Entekhabi and Brubaker (1995)).

All mentioned studies looked at land regions in isolation and prescribed advection from outside the domain. An exception to this is the simplified climate model of Entekhabi (1994) which was developed as a testbed for new parametrizations for General Circulation Models. This model consists of a land and ocean subdomain and regulates advection depending on the moisture difference between the two atmospheric columns. While their model is much more complex in its representation of the vertical structure, we will adopt here the idea of a coupled land-ocean-atmosphere system but restrict the scope to basic water balance equations with suitable empirical but physically motivated parametrizations for the moisture fluxes between the boxes. This approach allows us to analyze equilibrium solutions across the sensible parameter space, to put constraints on the ratio between mean land and ocean precipitation and to test the sensitivity of this ratio to the choice of model parameter values.

2. Model description

To understand the controlling factors and constraints for precipitation partitioning between land and ocean, we propose a box model as sketched in Figure 1. The model consists of an ocean subdomain denoted by subscript 'o', and a land subdomain denoted by 'ℓ' whose sizes are determined by the full domain length L and land fraction α. Each subdomain contains a ground box at the bottom (ocean or land) and an atmospheric box aloft. Their vertical extents are assumed infinite in downward and upward direction, respectively. In the horizontal direction, the model has periodic boundary conditions which makes it a closed system in which water is conserved. Such a *closed* model (CM) is suitable to describe the entire Earth or – if net moisture exchange with the extratropics is negligible – the tropics. In section 6, we discuss an *open* model (OM) version which allows for nonzero net advection from outside the model domain.

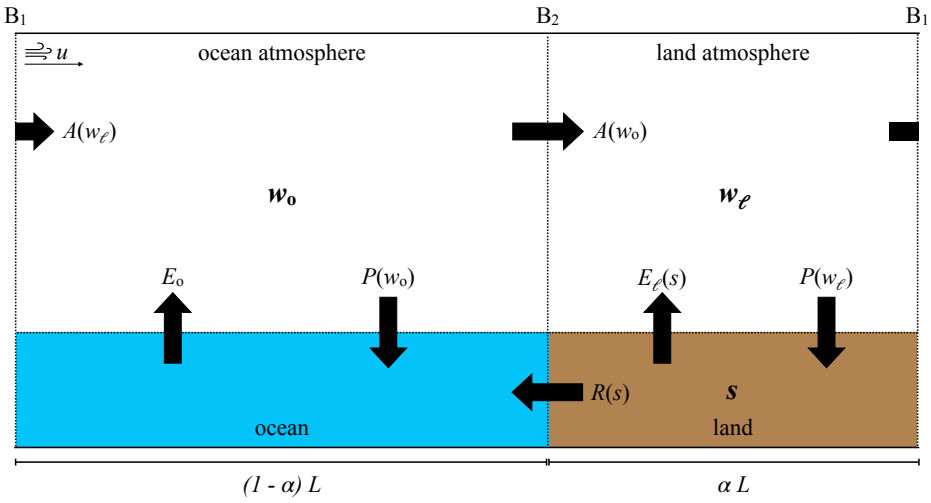

FIG. 1. Model sketch of the land-ocean-atmosphere system with periodic boundary conditions. Black arrows represent the box-averaged water fluxes between the four model boxes. With the exception of ocean evaporation E_o, which is treated as a constant model parameter, all fluxes are functions of the relative soil moisture saturation, s, or water vapor passes of land and ocean atmospheres, w_ℓ and w_o, respectively. The atmospheric moisture transport is driven by a constant horizontal background wind speed, u.

a. Water balance equations

To formulate the underlying water balance equations, we express all moisture fluxes between the boxes as functions of the system's moisture state. For atmospheric boxes, the moisture state is given by the mean water vapour pass w in mm, and for the land box by the unitless mean relative soil moisture saturation s. Since the ocean does not dry out, it does not require a moisture variable. Hence, the full information on the moisture state of the land-ocean-atmosphere system at any moment in time t is given by the set of state variables $\{w_o(t), w_\ell(t), s(t)\}$.

The time-evolution of the state variables is expressed by coupled water balance equations in which the water fluxes represent moisture sinks and sources (see e.g. Brubaker et al. (1991)):

$$\frac{ds}{dt} = \frac{1}{nz_\mathrm{r}}\left[P(w_\ell) - R(s, w_\ell) - E_\ell(s)\right] \tag{1}$$

$$\frac{dw_\ell}{dt} = E_\ell(s) - P(w_\ell) + A_\ell(w_\ell, w_\mathrm{o}) \tag{2}$$

$$\frac{dw_\mathrm{o}}{dt} = E_\mathrm{o} - P(w_\mathrm{o}) + A_\mathrm{o}(w_\ell, w_\mathrm{o}). \tag{3}$$

Note that the time-dependence of s, w_ℓ and w_o is implicit in Equations (1) to (3). The relevant fluxes, indicated by black arrows in Figure 1, are precipitation P, land evapotranspiration E_ℓ, ocean evaporation E_o, soil runoff R, and atmospheric advection A. The advection terms A_ℓ and A_o in Eqs. (2) and (3) represent the *net* advection rates into the land and ocean atmosphere, respectively, and are positive for net moisture import and negative for net moisture export. In a closed system, the domain-mean advection vanishes, i.e. $\alpha A_\ell + (1-\alpha)A_\mathrm{o} = 0$. All fluxes are given as spatial mean flux rates in mm day^{-1}. Dimensionless soil porosity n and hydrologically active soil depth z_r in mm are combined to one parameter.

b. Empirical relationships for water fluxes

To solve the water balance equations (1) - (3), we need expressions for the water fluxes. While the conservation of water is a fundamental condition, there are no simple fundamental laws governing the moisture exchange between the model boxes. Instead, we use empirical relationships, as has been done, for instance, by Rodriguez-Iturbe et al. (1991). As in their study, we express runoff as the fraction R_f of precipitation that does not infiltrate into the soil,

$$R(s, w_\ell) = R_\mathrm{f}(s)P(w_\ell), \tag{4}$$

with

$$R_\mathrm{f}(s) = \epsilon s^r, \tag{5}$$

and the two dimensionless parameters ϵ and r. Equation (5) tells us that runoff intensifies as the soil moistens.

For precipitation, Rodriguez-Iturbe et al. (1991) followed the approach of Budyko and Drozdov (1953) which assumes that the advected part of land precipitation is known. This is not a desirable

assumption in our case where the focus is on the factors controlling the land-to-ocean precipitation ratio which requires a free interaction between the two subdomains. Instead, we parametrize precipitation as a function of w, as established by Bretherton et al. (2004),

$$P(w) = \exp\left[a\left(\frac{w}{w_{\mathrm{sat}}} - b\right)\right]. \tag{6}$$

Equation (6) introduces two dimensionless parameters a and b and the saturated water vapor pass w_{sat} in mm.

The qualitative dependence of evapotranspiration on soil moisture saturation is long-known, see e.g. Budyko (1956). Seneviratne et al. (2010) present a schematic, where E_ℓ is close to zero for soil moisture values below the permanent wilting point, $s < s_{\mathrm{pwp}}$, increases approximately linearly in a transition range between the permanent wilting point and a critical value close to the field capacity, $s_{\mathrm{pwp}} < s < s_{\mathrm{fc}}$, and reaches a plateau for higher s-values, $s > s_{\mathrm{fc}}$, where evapotranspiration is nearly constant at its potential rate e_{p}. For computational convenience, we parametrize evapotranspiration by the following smooth function which has the qualitative properties described above,

$$E_\ell(s) = \frac{e_{\mathrm{p}}}{2}\left[\tanh\left(10\left(s - \frac{s_{\mathrm{pwp}} + s_{\mathrm{fc}}}{2}\right)\right) + 1\right]. \tag{7}$$

Unlike the land, the ocean is always fully saturated and we assume the resulting ocean evaporation rate to be a constant model parameter $E_{\mathrm{o}} = e_{\mathrm{o}}$.

It remains to find expressions for the *mean net* advection rates for the land and ocean atmospheres, hereafter just land/ocean advection. The total net advection into a given box is the difference between the moisture entering and leaving the box per unit time which is computed from the windward and leeward boundary water vapor pass times mean horizontal wind speed u in m s^{-1} (or mm day^{-1} for computations), respectively. Because we assume one uniform w across each atmospheric box, the wind transports the moisture amount $w_{\mathrm{o}}u$ from ocean to land and $w_\ell u$ from land to ocean. For the advection rates *per unit length* in mm day^{-1}, this gives

$$A_\ell = \frac{(w_{\mathrm{o}} - w_\ell)u}{\alpha L} = \frac{(w_{\mathrm{o}} - w_\ell)}{\alpha}\tau \tag{8}$$

for land advection and

$$A_{\mathrm{o}} = -\frac{(w_{\mathrm{o}} - w_\ell)u}{(1-\alpha)L} = -\frac{(w_{\mathrm{o}} - w_\ell)}{(1-\alpha)}\tau, \tag{9}$$

for ocean advection. On the right hand sides of Eqs. (8) and (9), we introduced the atmospheric transport parameter $\tau = u/L$ in day^{-1}. Its inverse value τ^{-1} represents a characteristic timescale for atmospheric transport. Similar concepts were used by Brubaker et al. (1991), Sobel and Bellon (2009), and Lintner et al. (2013) to model advection.

c. Parameter ranges

The chosen ranges for all free model parameters are provided in Table 1. These ranges constitute the parameter space throughout which we constrain the precipitation partitioning and test its sensitivity to parameter choices.

The ranges for s_{pwp} and s_{fc} are taken from data for different soil types presented in Hagemann and Stacke (2015), where we discard the extreme cases of pure sand and peat. After converting the provided volumetric data to relative soil moisture saturation values, s_{pwp} ranges between 0.15 and 0.55. We notice the fairly consistent relationship, $s_{\mathrm{fc}} = s_{\mathrm{pwp}} + 0.3$, and use it to reduce the number of free model parameters by one. Entekhabi et al. (1992) provide values for e_{p}, nz_{r}, r, and ϵ for both a semihumid and a semiarid climate. We take the values from these two climates as limits for the respective parameter ranges and vary e_{p} between 4 and 6 mm day^{-1} and nz_{r} between 50 and 120 mm. Entekhabi et al. (1992) set $r = 6$ for both cases but we let the runoff exponent range between 2 and 6, motivated by Rodriguez-Iturbe et al. (1991) who used $r = 2$ in an illustrative example. Since both studies agree on $\epsilon = 1$, we vary this parameter only slightly between 0.9 and 1.1. The precipitation parameters are taken from Bretherton et al. (2004) (where our b is called r). We use their fitting parameter values for monthly data as lower bounds for a and b, and the values for daily data as upper bounds. Bretherton et al. (2004) also give a typical value, $w_{\mathrm{sat}} = 72$ mm, for regions of tropical convection and we deem it appropriate to vary w_{sat} between 65 and 80 mm. Ocean evaporation can be constrained from observed latent heat fluxes. For instance, Kumar et al. (2017) find the mean flux of latent heat from tropical ocean surfaces to lie around 75 W/m^2 while an earlier study by Zhang and McPhaden (1995) indicates higher values of about 100 W/m^2. Based on these findings, we let e_{o} range between 2.5 and 3.5 mm day^{-1}. Lastly, τ is constrained by computing the smallest and largest value of u/L, respectively, where we assume plausible wind

speeds in the lower troposphere between 1 and 10 m s^{-1}, and let the domain length vary between 1000 and 40000 km, the upper limit corresponding to Earth's equatorial circumference. Thus, we obtain a range for τ between about 0.002 and 0.864 day^{-1}. Brubaker et al. (1991), whose transport parameter is equivalent to our $\alpha\tau^{-1}$, analyzed two regions centered on the Atlantic coast of the Amazon basin with a land fraction of about 0.5. From observations, they estimated monthly values for their transport parameter which translate to τ values between 0.01 and 10 – a range that is qualitatively similar to ours considering their rather small domain size.

d. Model assumptions

The simplicity of the proposed model owes to a number of assumptions, some of which are important to be made explicit. Foremost, we assume that each model box has well-mixed physical properties so that all interactions are adequately described in terms of spatial mean quantities. Second, we assume that the atmospheric and soil water storage does not change with time on large enough temporal and spatial scales which implies that the state of the land-ocean-atmosphere system is steady and that it is sufficient to analyze equilibrium solutions to Eqs. (1) to (3). Third, we determine the system's moisture state by water balance equations only, ignoring the potential effects of energy balance considerations such as the influence of a diurnal cycle. Energetic conditions are kept constant and only enter indirectly through values of energy-dependent parameters such as e_o or w_{sat}. Fourth, we prescribe a background wind speed with only a horizontal, constant component. Last, we assume that the functional relationship between precipitation and water vapor pass from Eqn. (6) holds over both land and ocean with the same choice of parameter values.

3. Methodology

Here, we present the different analysis methods that are employed to evaluate the model behavior and to assess the sensitivity of precipitation partitioning to variations of the parameter values. Precipitation partitioning is quantified by the land-to-ocean precipitation ratio,

$$\chi = \frac{P_\ell}{P_o} = \frac{P(w_\ell)}{P(w_o)}. \tag{10}$$

The equilibrium solution to the model equations (1) to (3) has to be found numerically. We use the DynamicalSystems.jl library from Datseris (2018) to find all roots of the model equations

TABLE 1. Parameter ranges for closed model simulations with uniform random sampling of parameter values.

Parameter	Minimum	Maximum	Range choice motivated by
s_{pwp}	0.15	0.55	Hagemann and Stacke (2015)
e_{p} [mm day^{-1}]	4.0	6.0	Entekhabi et al. (1992)
$nZ\mathrm{r}$ [mm]	50.0	120.0	Entekhabi et al. (1992)
e_{o} [mm day^{-1}]	2.5	3.5	Kumar et al. (2017), Zhang and McPhaden (1995)
ϵ	0.9	1.1	Rodriguez-Iturbe et al. (1991), Entekhabi et al. (1992)
r	2	6	Rodriguez-Iturbe et al. (1991), Entekhabi et al. (1992)
a	11.4	15.6	Bretherton et al. (2004)
b	0.5	0.6	Bretherton et al. (2004)
w_{sat} [mm]	65.0	80.0	Bretherton et al. (2004)
α	0.0	1.0	full possible range
$\tau = u/L$ [day^{-1}]	0.00216	0.864	plausible ranges for L and u

which represent stable fixed points of the system. Adopting an agnostic view on the plausibility of different combinations of parameter values from the ranges in Table 1, we perform 100 000 model simulations for randomly chosen points in the 11-dimensional parameter space, each yielding a corresponding equilibrium state and resulting fluxes. Scatter plots are used to analyze the sensitivity of χ to the different model parameters.

A suitable measure for the correlation between a parameter p_i and some quantity Q which accounts for the possibility of a non-linear and non-monotonic relationship between p_i and Q is their mutual information $MI(p_i, Q)$. Mutual information quantifies how much the knowledge of p_i reduces the uncertainty about Q. The mutual information of p_i and Q is computed as

$$MI(p_i, Q) = H(p_i) + H(Q) - H(p_i, Q), \tag{11}$$

where $H(p_i)$, $H(Q)$ and $H(p_i, Q)$ are the Shannon entropies of p_i and Q values, and of their joint distribution, respectively (Shannon (1948)). To enable a direct comparison of different parameter sensitivities, we rescale p_i and Q such that their values range between 0 and 1 and call the rescaled versions $\hat{p}_i$ and $\hat{Q}$. We use amplitude binning to ascribe probability distributions and follow the approach from Datseris and Parlitz (2022), p.106, to assess whether the obtained mutual information values are significantly different from the null-hypothesis of uncorrelated $\hat{p}_i$ and $\hat{Q}$. From the mutual information values of 10 000 shuffled surrogates of $\hat{p}_i$ and $\hat{Q}$, we compute a probability distribution of MI values for the uncorrelated case and define $MI_{\mathrm{uncorr},3\sigma}(\hat{p}_i, \hat{Q})$ as the

value that deviates by three standard deviations σ from the mean of this distribution. The mutual information index,

$$I_{MI}(p_i, Q) = \frac{MI(\hat{p}_i, \hat{Q})}{MI_{\text{uncorr},3\sigma}(\hat{p}_i, \hat{Q})}, \tag{12}$$

can then be used to determine whether the actual mutual information $MI(\hat{p}_i, \hat{Q})$ is high enough to pass the significance threshold, $I_{MI} = 1$. The higher $I_{MI}(p_i, Q)$, the more sensitive Q is to a variation of parameter p_i.

4. Basic model behavior and implications for χ

In this section, we analyze the output of the 100 000 closed model simulations with different parameter choices, henceforth referred to as "CM data", with the aim of determining the range of possible equilibrium values of the precipitation ratio. We start by characterizing the obtained equilibrium states and associated moisture fluxes.

Figure 2 illustrates the characteristics of possible equilibria through probability density functions (PDF) of equilibrium soil moisture values in panel a) and b), and water vapor pass values for land and ocean atmospheres in panel c). In panel b), s is rescaled to $\tilde{s} = (s - s_{\text{pwp}})/(s_{\text{fc}} - s_{\text{pwp}})$ in order to locate the equilibrium values relative to the different regimes of evapotranspiration which are separated by dashed vertical lines. The bulk of all simulations equilibrates to intermediate soil moisture values between $s = 0.25$ and 0.75 with a sharp peak in the center part of the E_ℓ-transition regime around $\tilde{s} = 0.5$. Similarly, the atmospheres equilibrate to intermediate w_{o} and w_ℓ values between 40 and 50 mm, well below w_{sat}. As a matter of comparison, a value of $w = 48$ mm is often employed to distinguished the moist deep tropics with deep convection from the dry subtropics (Masunaga and Mapes (2020)). Figure 2 also shows that land and ocean exhibit similar atmospheric moisture states but that the land is slightly drier than the ocean.

Figure 3 shows rolling averages of the equilibrium fluxes from all simulations as functions of the equilibrium soil moisture saturation. Note that the ocean advection rate A_{o} has negative values in all solutions and is therefore multiplied by -1 to simplify the comparison of its magnitude with other fluxes. Figure 3 contains the entire CM data, i.e. solutions for all different combinations of parameter values. Therefore, one should not confuse the plotted curves with the well-defined parametrizations of the water fluxes as functions of s for a fixed set of parameter values.

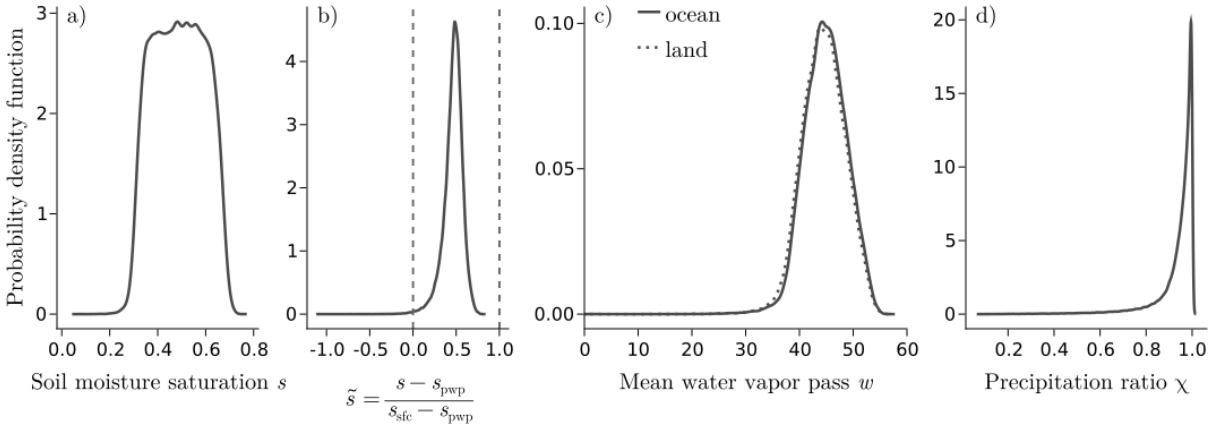

FIG. 2. Smoothed probability density functions of equilibrium soil moisture values in panel a), rescaled soil moisture values with vertical lines denoting the beginning and end of the transition regime of E_ℓ in panel b), water vapor pass of the land and ocean atmospheres in panel c) and values of the precipitation ratio in panel d).

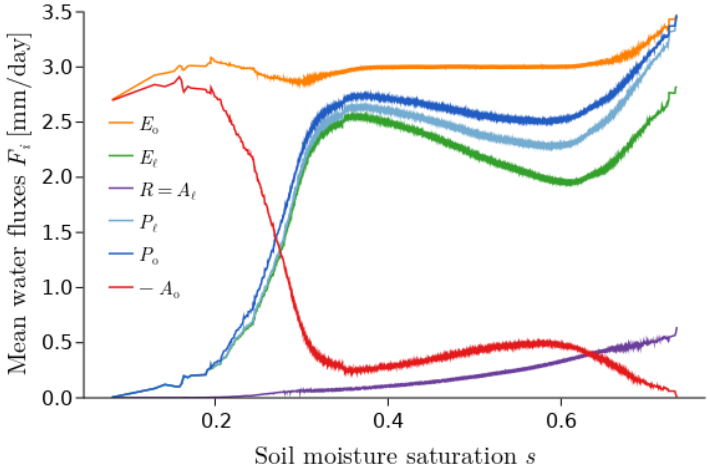

FIG. 3. Symmetric rolling average of equilibrium fluxes versus soil moisture saturation computed from CM data. For evapotranspiration (green line), the individual data points are shown as scatter plots and the range of $E_\ell(s)$ parametrizations for different parameter combinations is shaded in light green.

From Figure 3, we can draw first conclusions about the magnitude and relative importance of the fluxes in different regimes of equilibrium states as well as about the partitioning of precipitation in our simple land-ocean-atmosphere system:

1. Land advection, A_ℓ (purple line) is strictly positive, meaning that moisture is always supplied by the ocean atmosphere to the land atmosphere. In equilibrium, net advection to the land

compensates for soil runoff, i.e. $A_\ell = R$. This compensation mechanism in hydrological cycles is long-known, see e.g. Horton (1943) or Peixóto and Oort (1983), and has direct implications. According to the advection equations (8) and (9), net moisture transport from ocean to land requires the ocean atmosphere to be moister than the land atmosphere, $w_\mathrm{o} > w_\ell$. Since the same, monotonically increasing function $P(w)$ from Eqn. (6) is used over land and ocean, $P(w_\mathrm{o})$ is necessarily larger than $P(w_\ell)$. In other words, it rains more strongly over the ocean. This is confirmed by Fig. 3 where the dark blue curve for P_o always lies above the bright blue curve for P_ℓ. Hence, in our water balance model, an upper bound on the precipitation ratio exists, this upper bound being $\chi = 1$. That χ is bounded by one is also apparent from Fig. 2d) which shows the PDF of χ values. While the lower bound is essentially zero – for cases where land precipitation vanishes –, low values of χ are rare and 82.9 % of the parameter combinations yield values larger than 0.9, thereby falling into the range obtained by Hohenegger and Stevens (2022) from observations.

2. The ocean evaporation rate E_o (orange line) is always the largest flux. This can be explained as follows: E_o is partitioned into ocean precipitation P_o and ocean advection $|A_\mathrm{o}|$ so that each of these two components needs to be smaller than E_o. Since we know from the previous point that the land atmosphere is drier than the ocean atmosphere, it follows that $P_\ell < P_\mathrm{o} < E_\mathrm{o}$. Land precipitation can be written as the sum of evapotranspiration and runoff or evapotranspiration and advection so that again, each of these components needs to be smaller than E_o.

3. The shapes of the lines in Fig. 3 indicate that three soil moisture-precipitation regimes can be distinguished: For low soil moisture values up to $s \approx 0.36$, runoff and land advection are negligible and precipitation nearly equals evapotranspiration which rises sharply with s. In an intermediate soil moisture regime, $0.36 \lesssim s \lesssim 0.61$, precipitation decreases due to a strong negative trend of evapotranspiration. The precipitation decrease is slightly dampened by a steadily growing contribution from land advection (purple line). Lastly, above $s \approx 0.61$, precipitation increases again as the evapotranspiration trend reverses and advection keeps intensifying. Apparent contradictions such as the overall decline of advection out of the ocean atmosphere (red line) while advection into the land atmosphere is monotonically increasing or the decrease of evapotranspiration with increasing soil moisture in the intermediate regime

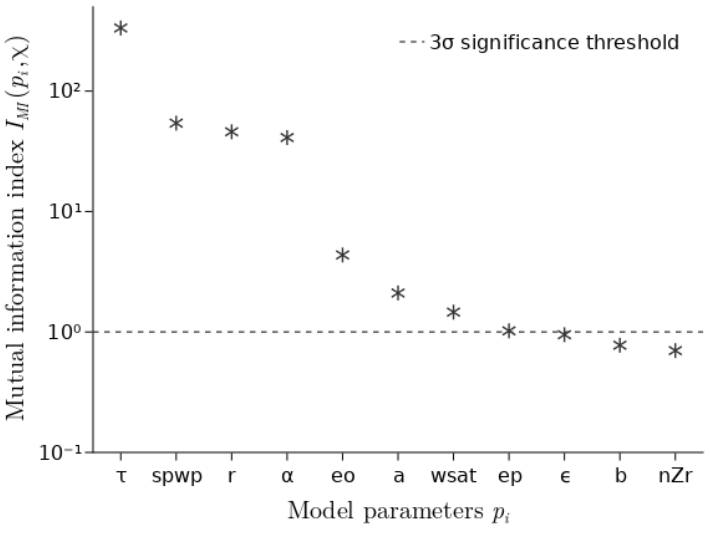

FIG. 4. Relative sensitivity of the precipitation ratio to the different model parameters p_i measured by the mutual information index I_{MI}. Values larger than $I_{MI} = 1$ (dashed line) lie above the significance threshold.

can be resolved by understanding the parameter sensitivities and how different parameters interact.

5. Parameter sensitivity of χ

Having established that χ is bounded between zero and one in our water balance model, we want to better understand the controls of different parameters on the attained precipitation ratio. To this end, we quantify the sensitivity of χ to each individual model parameter by the mutual information index $I_{MI}(p_i)$ defined in Eqn. (12). A comparison of the results for all model parameters p_i is provided in Figure 4. The atmospheric transport parameter τ is by far the most sensitive parameter, followed by the soil parameters permanent wilting point s_{pwp} and runoff exponent r, and the land fraction α. Some of the remaining parameters also have I_{MI}-values above or close to the significance threshold (dashed line) but we do not discuss them in detail due to their rather small contributions to the overall sensitivity.

a. Atmospheric transport parameter τ

Figure 5 shows scatter plots of the precipitation ratio versus the four most sensitive model parameters. The relationship between χ and τ in Fig. 5a) is strongly nonlinear and leads to

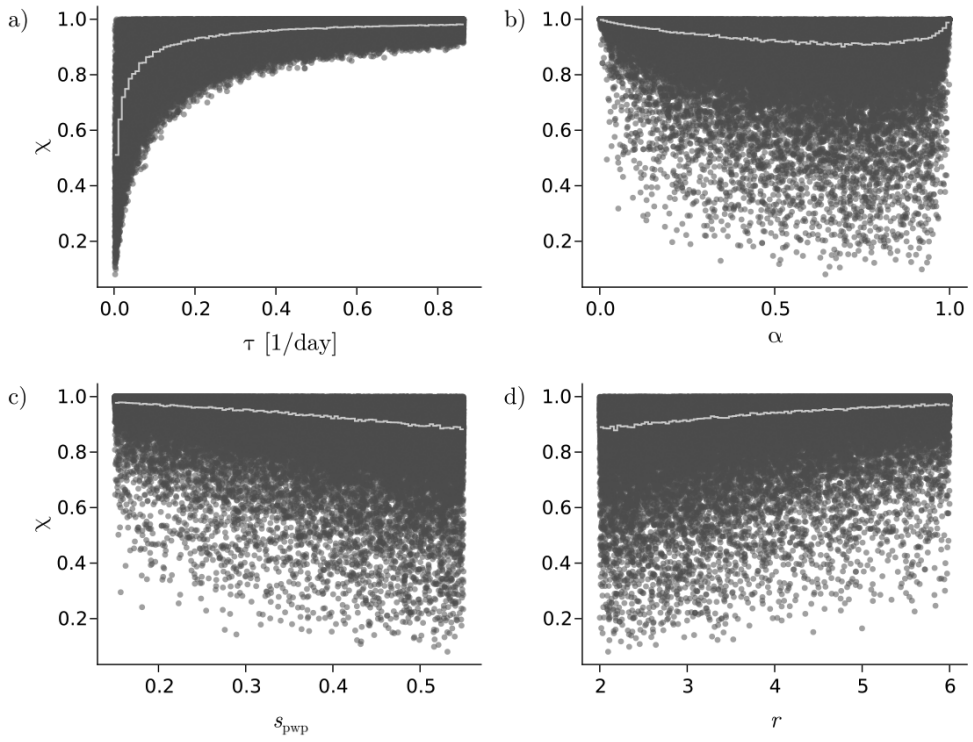

FIG. 5. Precipitation ratio χ versus atmospheric transport parameter τ, land fraction α, permanent wilting point s_{pwp} and runoff exponent r. The white lines show χ mean values computed for 100 bins along s_{pwp}.

variations of the χ mean value between 0.5 and 0.98, confirming the high sensitivity determined in the mutual information analysis. The precipitation ratio tends to be low for low values of τ and converges towards one as τ increases. As τ increases, the spread of χ values around the mean (white line) narrow, making τ a better predictor for the precipitation partitioning.

Physically, τ corresponds to the fraction of the domain length that moisture can travel horizontally in the atmosphere in one day. As such, it can be interpreted as an efficiency of atmospheric moisture transport. High values of τ imply a fast exchange of moisture between land and ocean atmospheres with the result of low moisture differences, $\Delta w = w_{\mathrm{o}} - w_{\ell}$, between the two. Since we assume the same precipitation parametrization $P(w)$ for land and ocean, small Δw means that the precipitation rates over land and ocean are similar and that χ is close to one. In contrast, small values of τ can sustain larger moisture differences between land and ocean and lead to smaller values of χ.

In fact, the distribution of data points in Fig. 5a) indicates that τ controls the lower limit of χ which increases with τ while the upper limit, $\chi = 1$, seems independent of τ and must therefore

be controlled by a different parameter. We can understand how τ determines the lower bound of the precipitation ratio by returning to the advection equations (8) and (9), each of which can be rephrased as the product of Δw and an advection efficiency, namely τ/α for land advection and $\tau/(1-\alpha)$ for ocean advection. Only if both advection efficiencies are low, a large moisture difference and low χ value can be sustained. The fact that α ranges between zero and one and that it affects ocean and land advection efficiencies in opposite ways suggests a "sweet spot" of overall low advection efficiency at $\alpha = 0.5$, leaving it to τ to set the final value of this lowest advection efficiency and thereby the lower bound of χ. In the next section, we will see that the complexity of land-atmosphere interactions leads to an asymmetry in the relationship between χ and α such that the postulated "sweet spot" of lowest χ is found at a larger land fraction than $\alpha = 0.5$.

b. Land fraction α

Fig. 5b) illustrates how α impacts the partitioning of precipitation. The χ mean varies between 0.91 and 1.0 on a u-shaped line between the extreme cases of an ocean-only, $\alpha = 0$, and land-only, $\alpha = 1$, scenario where in both cases χ is close to one. As for τ, the impact of land fraction changes on the precipitation ratio is rooted in their control on the advection efficiencies, τ/α and $\tau/(1-\alpha)$. However, the particular role of α is to differentiate between the efficiency of moisture export out of the ocean subdomain and the efficiency of moisture import into the land subdomain. If α is small, ocean advection is inefficient because the average time for oceanic water vapor to reach the land is long. In contrast, it takes only little time to distribute the imported moisture over the small land size so that land advection is efficient. The reverse applies for a large land fraction.

While the model cannot handle the endpoints of the α-range, we can examine them in a thought experiment: Imagine a domain fully covered by ocean. Water balance would require the ocean precipitation to balance ocean evaporation, $P_\mathrm{o} = E_\mathrm{o}$. If we now introduced an infinitesimal patch of land, some of the evaporated moisture would be advected into the tiny land atmosphere. Since τ/α is high, the atmospheric conditions would assimilate rapidly without significantly altering the moisture conditions over the vast ocean. Hence, for such small α, the system is expected to behave as if the land did not exist with overall moist atmospheric conditions and similarl land and ocean precipitation rates close to E_o. As the other extreme, imagine a pure land domain but with the assumption that runoff remains possible. The runoff would continuously reduce the soil moisture

saturation and with it evapotranspiration and precipitation until the trivial equilibrium solution $\{s = 0, w_\ell = 0\}$ was reached. Allowing for advection from an infinitesimal ocean would not change the picture much. With high efficiency $\tau/(1-\alpha)$, almost the entire but nevertheless small amount of evaporated oceanic moisture would be exported to the land, leaving behind a fairly dry ocean atmosphere and hardly affecting the dry state of the large land atmosphere and soil. Hence, the system would behave as if the ocean did not exist with similarly low precipitation rates close to zero in both subdomains.

The transition between the ocean-only and land-only scenario is best understood by examining the individual rain rates P_o and P_ℓ over the range of α as shown in Figure 6. The two extremes are connected by a regime of monotonic drying as the ocean surface – the only true source of moisture for the system's hydrological cycle – shrinks. Although not shown, the overall reduction of available moisture as the land fraction increases also manifests itself in a soil moisture decrease. We can investigate the shapes of P_ℓ and P_o theoretically, assuming all parameters except α to be fixed. Expressions for the rain rates are found by imposing equilibrium conditions on Eqns. (2) and (3), yielding

$$P_\ell = E_\ell(s(\alpha)) + \Delta w(\alpha)\frac{\tau}{\alpha} \tag{13}$$

$$P_\mathrm{o} = e_\mathrm{o} - \Delta w(\alpha)\frac{\tau}{1-\alpha}. \tag{14}$$

Note that $s(\alpha)$ and $\Delta w(\alpha)$ are implicit functions of the land fraction but that we lack analytical expressions for them. As α increases in Fig. 6, P_ℓ decreases more strongly than P_o because land precipitation is not only affected by (initially sharply) decreasing $1/\alpha$ but in addition by a reduction in evapotranspiration as s declines. In contrast, ocean precipitation is only reduced by (initially weakly) increasing advection. The additional influence of α on P_ℓ through E_ℓ causes the asymmetry of the $\chi(\alpha)$-mean in Figure 5b) with a minimum around $\alpha = 0.75$ instead of 0.5. Although $\chi(\alpha)$ is u-shaped for every combination of the other parameter values, the location of the minimum differs slightly. Generally, the width of the spread of χ values indicates that the land fraction is the dominant predictor for χ near its extreme values but that its influence weakens towards intermediate values.

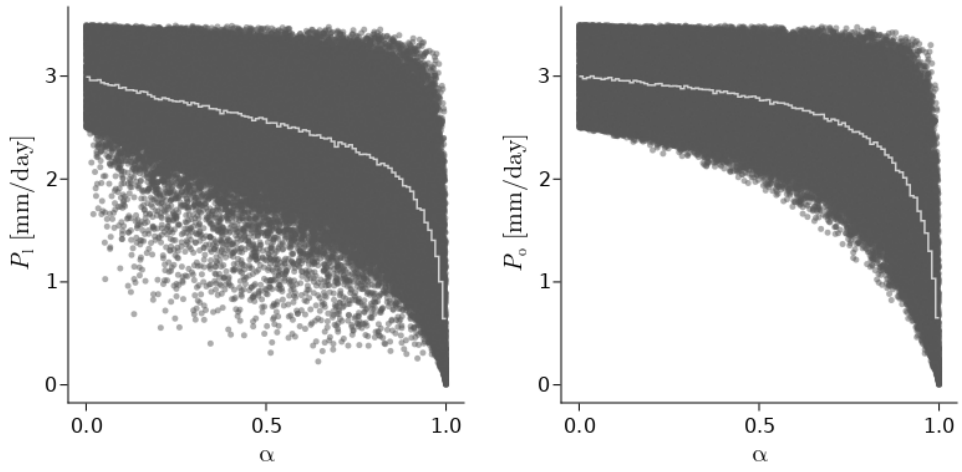

FIG. 6. Ocean precipitation rate P_o and land precipitation rate P_ℓ versus land fraction α. The transition from an ocean-only to a land-only model scenario is marked by a decrease of both precipitation fluxes, indicating overall moist conditions for small land fractions and dry conditions for large land fractions.

c. Permanent wilting point s_{pwp} and field capacity s_{fc}

Figure 5c) and 5d) show that variations in the soil parameters lead to mean variations of χ similar to the effects from land fraction changes, with the mean varying between $\chi = 0.88$ and 0.98. In Fig. 5c), the precipitation ratio shows an almost linear, negative trend as the permanent wilting point increases. To understand this trend, it is helpful to consider a system in equilibrium for some value of the permanent wilting point, e.g. $s_{\mathrm{pwp}} = 0.3$, and to examine how the system responds when this value is suddenly changed to $s_{\mathrm{pwp}} = 0.4$. The presented arguments assume that the other parameter values stay fixed when varying s_{pwp} but we can see from the right panel of Figure 7 that the influence of the permanent wilting point also leaves its imprint on the mean soil moisture state (white line) in the form of a clear positive trend. We therefore make use of the mean value for illustration purposes. The left panel of Figure 7 depicts the evapotranspiration curves for $s_{\mathrm{pwp}} = 0.3$ and 0.4, respectively, with fixed $e_{\mathrm{p}} = 5.0\,\mathrm{mm\,day^{-1}}$. Because s_{pwp} and s_{fc} are equidistant for different soil types, a change of s_{pwp} merely shifts the evapotranspiration curve along s.

The mean soil moisture value in the CM data for $s_{\mathrm{pwp}} = 0.3$ is $s = 0.45$. This initial state and its corresponding evapotranspiration value are displayed as blue dots in Figure 7. An abrupt increase of the permanent wilting point to $s_{\mathrm{pwp}} = 0.4$ leads to an instantaneous drop ΔE_{inst} in the evapotranspiration (first red arrow connecting the blue and green dots). The green dot represents

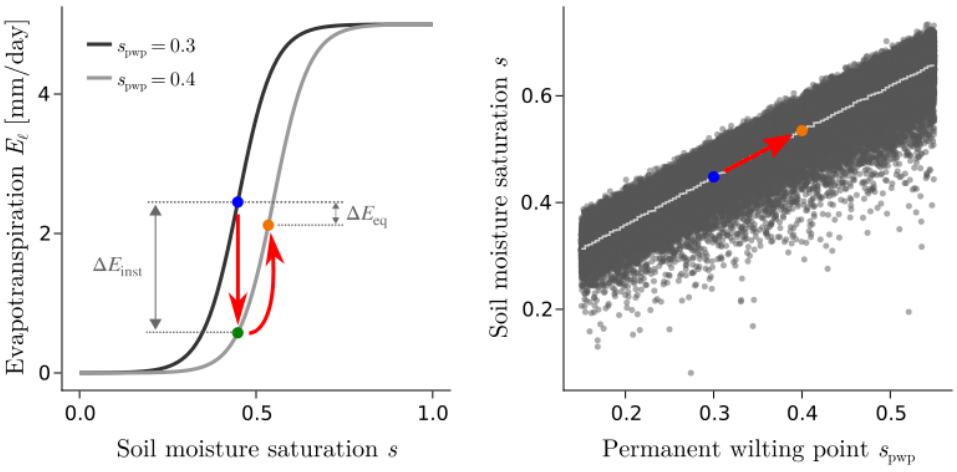

FIG. 7. Influence of an increase in s_{pwp} on the equilibrium state. Left: Higher values of s_{pwp} shift the graph of the E_ℓ parametrization towards larger s. Right: Equilibrium values of the soil moisture saturation from CM data plotted over s_{pwp} values. The blue dots mark the initial equilibrium state, the green dot represents a temporary state of soil moisture imbalance due to a sudden increase of s_{pwp} and the orange dot marks the the eventually attained equilibrium for the new s_{pwp} value.

a temporary state where the model is not in equilibrium because the state variables have not yet responded to the new situation in which the soil receives the same amount of precipitation but loses less water through evapotranspiration. Consequently, the soil moistens. As time progresses, the system attains a new equilibrium state (orange dot) at a higher s value. However, as the soil moistens, not only evapotranspiration but also runoff and, hence, land advection increase. With fixed τ and α, Δw has to increase to allow for increased advection. Since the ocean atmosphere needs to supply more moisture to the land, w_o decreases. Therefore, an increase in advection from increased Δw is only possible, if w_ℓ decreases more strongly than w_o. Accordingly, P_ℓ decreases more strongly than P_o which explains why χ declines with increasing s_{pwp}.

The new equilibrium is characterised by a moister soil with larger runoff but reduced precipitation, thus leaving less moisture to evapotranspiration. The new E_ℓ is by ΔE_{eq} smaller than its initial value. This response to changes in s_{pwp} is responsible for the counterintuitive shape of fluxes in Figure 3 for intermediate s values. Precipitation and evapotranspiration of moister soils are reduced while the mean value of s_{pwp} increases linearly (not shown).

d. Runoff exponent r

The relationship between χ and r in Figure 5d) resembles $\chi(s_{\mathrm{pwp}})$ but with opposite trend: χ increases with r while it decreases with s_{pwp}. Indeed, the similarity originates from a similar physical mechanism. In the formulation of the runoff fraction, $R_{\mathrm{f}} = \epsilon s^r$, r enters as the exponent. As for the s_{pwp}-dependence, we can think of the system in equilibrium, this time responding to a sudden increase of r. Runoff drops to a lower value and soil moisture begins to increase. As a consequence, also both atmospheres start to moisten: First, w_ℓ increases through increased evapotranspiration from the wetter soil, reducing the moisture difference between land and ocean. Second, the reduction of Δw implies reduced advection, allowing the ocean atmosphere to keep more moisture to itself, and w_{o} increases. Eventually, the decreasing advection matches the runoff which started to intensify again after the initial drop as the soil moistened. A new equilibrium is attained in which runoff is reduced compared to the initial state with lower r value. Equally reduced land advection with lower Δw reflects assimilated atmospheric moisture conditions and, hence, increased χ.

Equilibrium states with higher r value also have stronger precipitation rates from higher w_ℓ and w_{o}. In Figure 3, we see the influence of r in both the low and high soil moisture regime, where it works in tandem with the land fraction to shape the moisture fluxes. Both precipitation increases for low and high s, respectively, are caused by a combination of increasing r and decreasing α.

6. Under which circumstances can χ become larger than 1?

So far, we concluded that the precipitation ratio is bounded by an upper limit of one due to the necessity of net moisture transport from ocean to land and the assumption that the efficiency with which atmospheric moisture is turned into precipitation is the same over land and ocean. However, we know of local systems in the real world for which higher rain rates are observed over land compared to the adjacent ocean. For instance, Qian (2008), Sobel et al. (2011), Cronin et al. (2015), Wang and Sobel (2017) and Ulrich and Bellon (2019) found precipitation enhancement over tropical islands and attributed this observation mainly to the development of sea breezes triggering precipitating convection over the islands. Even for the full tropics, some observational datasets suggest a precipitation ratio slightly larger than one (Hohenegger and Stevens (2022)). For the tropical land fraction, $\alpha \approx 0.35$, our model gives a mean ratio of 0.94 which falls within

the range of observational values. Yet, ratios of individual simulations reach as low as $\chi = 0.08$, mostly due to low τ values. Hence, the model tends to underestimate the actual precipitation ratio and it cannot produce values larger than one. In the following, we explore different ways in which our model framework could me modified to enable precipitation enhancement over land, i.e. $\chi > 1$.

a. Relaxing assumptions of the closed model

The first direct limitation for the precipitation ratio is the assumption that the different surface characteristics of land and ocean do not affect the way it rains. For a given water vapor path, it rains the same amount over land and ocean. While we can expect a moister atmosphere to yield more rainfall, the exact shape of $P(w)$ might differ for different surfaces. While Ahmed and Schumacher (2017) found different shapes for land and ocean precipitation, Schiro et al. (2020) did not confirm a distinct difference, leaving the picture inconclusive. If different parametrizations $P_\ell(w)$ and $P_\mathrm{o}(w)$ were used for land and ocean precipitation, respectively, and $P_\ell(w)$ was larger than $P_\mathrm{o}(w)$ in the relevant range of w-values, it is conceivable that an equilibrium state could exhibit a moister ocean atmosphere supporting net advection to the land and at the same time stronger land precipitation, so that $\chi > 1$.

Second, we treat all model boxes as being homogeneous and well-mixed which allows us to work with mean fluxes rather than resolving the horizontal direction explicitly. It is well-known that an airstream traversing an oceanic region will moisten along its trajectory since mean ocean evaporation typically exceeds mean ocean precipitation and the reverse applies to land regions. Ogino et al. (2016) and Ogino et al. (2017) further found that the conventional view in which Earth's surface gets divided into ocean and land misses out on particular interactions driven by the land-sea contrast which are confined to a coastal region, a few hundred kilometers seaward and landward from the coast. These coastal regions receive more rain than both the open ocean and inland continental regions. Also Bergemann and Jakob (2016) found that tropical rainfall over land associated with coastal effects such as sea breezes can occur under drier atmospheric conditions than rainfall over the open ocean. Hence, adding coastal zones with a specific coastal precipitation parametrization to the model is another flavor of the argument that – for precipitation enhancement over land – it has to rain differently in different subdomains. Coastal zones might also capture the

fact that precipitation enhancement is particularly strong over relatively small land masses where coastal effects are expected to be more influential.

Third, the model does not account for diurnal variations of the energy budget. As a consequence, diurnally forced phenomena like sea breezes which tend to enhance precipitation over land are not captured. Energy-dependence can be implemented in different ways – either fundamentally by coupling water balance and energy balance equations, or indirectly by expressing energy-dependent parameters such as τ, e_o or w_{sat} as functions of time which exhibit a distinct diurnal cycle over land and over ocean. Even with the same $P(w)$ across the domain, a diurnal cycle may lead to $\chi > 1$ if the increased moisture transport to the land during the day leads to higher temporary rain rates over land than over ocean, and if the reverse transport during the night does not fully compensate for the daytime precipitation signal. In other words, the diurnal cycle may explain why precipitation ratios are close to one and can be larger than one in reality.

Last, our model configuration with one land and one ocean box makes the comparison with observed values difficult. It is likely that a different land distribution with more boxes would lead to higher precipitation ratios because of increased advection efficiencies for smaller boxes. If, in addition, the boxes were differently sized, we might see instances where $\chi > 1$. In equilibrium, each ocean atmosphere would still be moister than the leeward land atmosphere but it cannot be precluded that weighting the precipitation rates by the different box sizes would yield higher mean land than ocean precipitation.

b. Opening the closed model

The previous arguments still treat the land-ocean-atmosphere system as a closed model. This assumption may be valid over the full tropics, assuming a negligible net moisture exchange with the extratropics, but it is certainly invalid over islands, where land precipitation enhancement is typically observed. Hence, allowing for atmospheric inflow and outflow out of the domain might permit land-to-ocean precipitation ratios larger than one. We test this hypothesis in two ways.

First, moisture import or export from an external environment outside the model boundaries can be incorporated by an additional advection term, A_{ext} in mm day^{-1} in Equation (3) for oceanic water vapor. A positive A_{ext} denotes inflow of external moisture, while a negative A_{ext} means that the ocean atmosphere loses moisture through the model boundaries. This construction mimics

the case of an island surrounded by an ocean under the influence of lange-scale convergence or divergence. But is this change in the model framework sufficient to create scenarios for which $\chi > 1$?

We argue that the answer is no: Regardless of whether the system is gaining or losing moisture through its boundaries, an equilibrium state still requires a net transport of moisture from ocean to land, and therefore $w_o > w_\ell$ with $\chi < 1$. The term A_{ext} acts in a similar fashion as ocean evaporation. Under the influence of moisture convergence, the positive A_{ext} is equivalent to an increase in E_o and merely increases the moisture content in all boxes. In the case of moisture divergence, negative A_{ext} acts like a reduction of E_o and an overall drier equilibrium state is attained as long as $|A_{ext}| < E_o$. If the loss through the model boundary is stronger than the moisture input from the ocean surface, the system will undergo drying until the trivial solution $\{w_o = 0, w_\ell = 0, s = 0\}$ is reached.

Second, we can also open the model by allowing moisture to enter the domain from one side and leave it on the other side. As an illustrative example for this type of *open model*, we consider the simplest configuration with a land box of length L_ℓ, placed between two equally big ocean boxes of lengths $L_{o1} = L_{o2}$. The subscript 'o1' refers to the ocean in front of the island as seen by the airflow horizontally traversing the domain at constant wind speed, while 'o2' refers to the ocean behind the island. The equations governing the evolution of w_{o1}, w_ℓ and w_{o2} and s are formulated in analogy to the closed model equations and can be found in Appendix A along with a model sketch. This open model requires an additional parameter w_0 for the windward boundary water vapor pass which can range between zero and w_{sat}. As for the closed model, we perform 100 000 simulations with randomly chosen combinations of parameter values from Table 1 with the modification that the full domain length is varied between 200 and 2000 km. The obtained set of equilibrium solutions is refer to as "OM data".

The precipitation ratio is now defined in terms of mean precipitation rates $\bar{P}_\ell$ and $\bar{P}_o$ as

$$\chi_{om} = \frac{\bar{P}_\ell}{\bar{P}_o} = \frac{2P_\ell}{P_{o1} + P_{o2}}. \tag{15}$$

As in the case of the closed model, equilibrium can only be attained if the land atmosphere receives advected moisture from the ocean. In the open model, this means that the first ocean atmosphere has to be moister than the land atmosphere which – sticking to the assumption of the same parametrization for precipitation across the domain – implies $P_{o1} > P_\ell$. It follows from

Equation (15) that a precipitation ratio larger than one is possible if the inequality, $P_{o2} < 2P_\ell - P_{o1}$, is fulfilled. This means, the second ocean atmosphere must be dry enough to compensate for the relatively moist first ocean atmosphere, such that the mean ocean precipitation is smaller than P_ℓ. From the OM data, we find that only about 6.7 % of all simulations meet this condition and yield $\chi_{om} > 1$. As expected, these simulations have in common that atmospheric moisture reduces along the wind trajectory, i.e. $w_0 > w_{o1} > w_\ell > w_{o2}$.

We perform the same sensitivity analysis as for the closed model to understand which parameter combinations lead to ratios larger than one and to which parameters χ is most sensitive. Opening the model does not fundamentally change the principal sensitivities but modifies their order of importance: The most sensitive parameter is now w_0 with $I_{MI}(w_0, \chi) = 254$, followed by α with $I_{MI}(\alpha, \chi) = 202$ and τ with $I_{MI}(\tau, \chi) = 147$. All other parameters, including the formerly relevant soil parameters, have I_{MI} values lower than 8 and can be neglected as predictors for χ. To understand which parameter combinations lead to $\chi > 1$, Figure 8 shows PDFs of the values of w_0, α and τ for simulations with precipitation ratios smaller and larger than one in blue and orange, respectively. Even though the distributions have a significant overlap, $\chi > 1$ requires a large enough boundary water vapor pass $w_0 \gtrsim 38$ mm and becomes more likely with smaller land fraction. States with $\chi > 1$ do not exist for $\alpha > 0.93$ and are most likely around $\alpha = 0.05$. In contrast, a value of $\chi > 1$ seems to be possible with any value for τ. Further inspection of the state variable values (not shown) reveals that equilibrium states with $\chi > 1$ are overall moist. Soil moisture saturation values cluster close to and beyond the field capacity. Water vapor pass values peak around 48 mm and get no lower than 38 mm. Simulations with $\chi < 1$, in contrast, exhibit equilibrium states across the entire moisture spectrum, including very dry states with soil moisture values below the permanent wilting point.

As in the case of the closed model, the open model results are subject to the choice of the land distribution and may change for different numbers of land boxes. In addition, the open model is sensitive to the location of the land box which affects the relative size of the two ocean boxes. However, a test of different asymmetric configurations indicates that the presented statements are only affected quantitatively, not qualitatively.

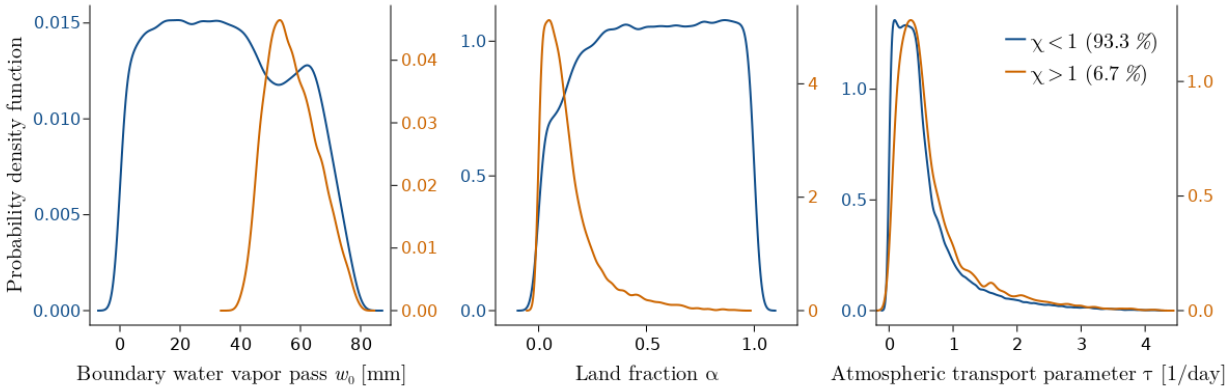

FIG. 8. Probability density functions of parameter values for w_0, α and τ. Blue and orange graphs contain data from simulations with precipitation ratios smaller and larger than one, respectively. Ratios larger than one are only found for 6.7 % of all simulations.

7. Conclusions

This study was motivated by our lack of theoretical understanding of how Earth's total precipitation gets partitioned between land and ocean. Estimates of the ratio between spatially averaged land and ocean precipitation rates, $\chi = P_\ell / P_o$, from different observational datasets range between 0.9 and 1.04 Hohenegger and Stevens (2022). We wanted to know which atmospheric and land processes determine the partitioning and what constraints can be set on χ based on water balance equations.

We introduced a conceptual box model that describes the rate of change of soil moisture and atmospheric moisture over ocean and land, respectively. The water balance components are expressed by empirical parametric functions of the mean water content of the land and atmospheric boxes. In particular, as a null hypothesis, we assumed that precipitation increases exponentially with water vapor path and that the presence of land does not affect this relationship. In order to investigate the bounds of χ and its parameter sensitivity, we analyzed a large number of equilibrium solutions for different combinations of model parameter values. The obtained results for the case of a closed model with one land and one ocean box can be summarized as follows:

- As long as the land does not affect the relationship between precipitation and water vapor path, the precipitation ratio is bounded by an upper limit of one. This is a direct consequence of the equilibrium condition that the land's loss of water through runoff needs to be compensated

for by an equally large net atmospheric moisture transport from a moister ocean atmosphere to a drier land atmosphere.

- The lower limit of χ is zero in cases where the land precipitation is zero. Although χ can theoretically vary between zero and one, values between 0.75 and 1.0 appear most likely, with 95 % of the simulations falling into this range.

- The free model parameters are listed in Table 1. We find that χ is most sensitive to a variation of the atmospheric transport parameter τ, followed by the two soil parameters permanent wilting point s_{pwp} and runoff exponent r, and land fraction α. Efficient atmospheric transport, represented by high τ, helps to assimilate the land and ocean atmospheres and yields high values of χ. Land fraction is most influential near its extreme values, $\alpha \to 0$ and $\alpha \to 1$, where in both cases χ is close to one. Near these extremes, the highly efficient advection rate into or out of the respective tiny land or ocean atmosphere causes the atmospheric conditions in both boxes to assimilate. Finally, χ decreases with increasing permanent wilting point and increases with decreasing r. This can be understood from the way in which these parameters control the amount of runoff and thereby the demand for advective moisture inflow into the land subdomain. With τ and α held constant, the advective inflow is regulated by the moisture difference Δw whose change is directly related to a change of χ in the same direction.

- The closed water balance model tends to underestimate the precipitation ratio. For a land fraction similar to the tropics and a domain length of 40000 km, an expected ratio of 0.6 is obtained which is lower than any of the values obtained by Hohenegger and Stevens (2022). It also cannot explain observed island precipitation enhancement as reported by other studies because χ is bounded by one. Given the assumptions of our model, our interpretation of this finding is that precipitation enhancement over land requires the land to affect the relationship between precipitation and water vapor pass, that precipitation enhancement is linked to the presence of a diurnal cycle, that a different land distribution is required, or that it is only possible in an open model which allows for net advection into or out of the domain. We tested this last option with a model configuration in which moisture can enter the model through the windward boundary and leave on the other side. For this setup, precipitation ratios larger than one exist for a small subset (6.7 %) of the performed simulations. These cases require a large

moisture inflow with a boundary water vapor pass of at least 38 mm day^{-1}, and small land sizes, typically around $\alpha \approx 0.05$ and no larger than $\alpha = 0.93$.

Even though the simple conceptual model does not capture the full range of physical processes that influence the precipitation partitioning between land and ocean, it is able to constrain the precipitation ratio and identifies the efficiency of atmospheric transport as the dominant factor governing the partitioning, while other parameters such as the soil type are shown to be less influential. Its limitations show that the presence of a diurnal cycle is indispensable for capturing the interaction between precipitation and rather small land masses and that land is likely to change the precipitation efficiency compared to over the ocean.

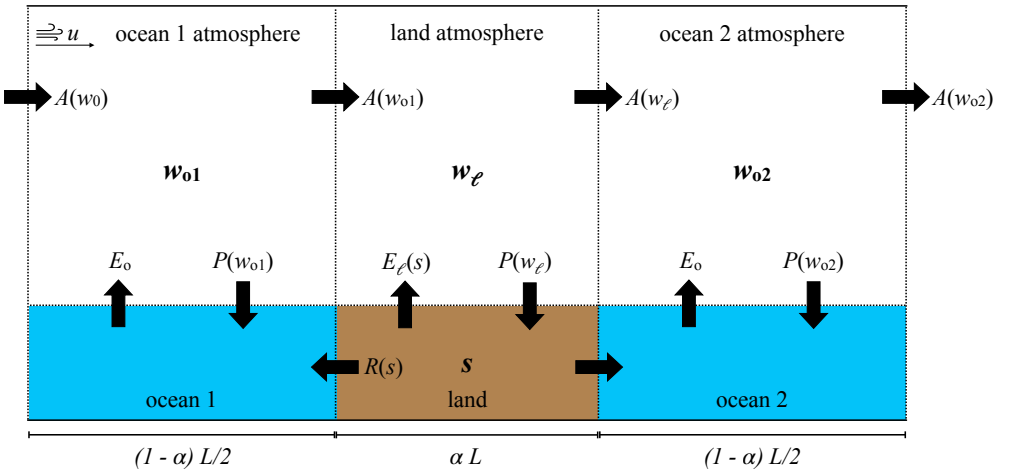

FIG. A1. Sketch of an land-ocean-atmosphere system consisting of an island between two ocean boxes with respective atmospheric boxes aloft. The lateral model boundaries are open, allowing moisture to enter and leave the modelled domain. The water vapor pass value at the windward model boundary is given by parameter w_0 and may reflect synoptic scale atmospheric conditions. Moisture fluxes between boxes are analogous to the closed model described in Section 2.

APPENDIX A

Open model formulation

The equations governing an open model configuration with an island (subscript 'ℓ') between two ocean boxes (subscripts 'o1' and 'o2' in the order of their appearance along the wind trajectory) are similar to the ones for the closed model introduced in Section 2. However, four instead of three equations are needed,

$$\frac{ds}{dt} = \frac{1}{nz_r}\left[P(w_\ell) - R(s, w_\ell) - E(s)\right] \tag{A1}$$

$$\frac{dw_{o1}}{dt} = E_o - P(w_{o1}) + \frac{(w_0 - w_{o1})u}{L_{o1}}. \tag{A2}$$

$$\frac{dw_\ell}{dt} = E(s) - P(w_\ell) + \frac{(w_{o1} - w_\ell)u}{L_\ell} \tag{A3}$$

$$\frac{dw_{o2}}{dt} = E_o - P(w_{o2}) + \frac{(w_\ell - w_{o2})u}{L_{o2}},. \tag{A4}$$

The lengths of the model subdomains can be written as $L_{o1} = L_{o2} = (1-\alpha)L/2$ and $L_\ell = \alpha L$, where L denotes the full model domain length.

For a small number of parameter combinations, no equilibrium solution to the open model equations could be determined.

Acknowledgments.

Data availability statement.

References

Ahmed, F., and C. Schumacher, 2017: Geographical differences in the tropical precipitation-moisture relationship and rain intensity onset. *Geophysical Research Letters*, **44 (2)**, 1114–1122, https://doi.org/10.1002/2016GL071980, URL https://onlinelibrary.wiley.com/doi/abs/10.1002/2016GL071980.

Bergemann, M., and C. Jakob, 2016: How important is tropospheric humidity for coastal rainfall in the tropics? *Geophysical Research Letters*, **43 (11)**, 5860–5868, https://doi.org/10.1002/2016GL069255, URL https://onlinelibrary.wiley.com/doi/abs/10.1002/2016GL069255.

Bretherton, C. S., M. E. Peters, and L. E. Back, 2004: Relationships between water vapor path and precipitation over the tropical oceans. *J. Climate*, **17**, 1517–1528, https://doi.org/10.1175/1520-0442(2004)017<1517:RBWVPA>2.0.CO;2.

Brubaker, K., D. Entekhabi, and P. Eagleson, 1991: Atmospheric water vapor transport: Estimation of continental precipitation recycling and parameterization of a simple climate model. URL https://ntrs.nasa.gov/citations/19910018381.

Brubaker, K. L., and D. Entekhabi, 1995: An analytic approach to modeling land-atmosphere interaction: 1. construct and equilibrium behavior. *Water Resources Research*, **31 (3)**, 619–632, https://doi.org/10.1029/94WR01772, URL https://agupubs.onlinelibrary.wiley.com/doi/abs/10.1029/94WR01772.

Brubaker, K. L., D. Entekhabi, and P. S. Eagleson, 1993: Estimation of continental precipitation recycling. *Journal of Climate*, **6**, 1077–1089, https://doi.org/10.1175/1520-0442(1993)006<1077:EOCPR>2.0.CO;2, URL https://journals.ametsoc.org/jcli/article/6/6/1077/39303/Estimation-of-Continental-Precipitation-Recycling.

Budyko, M. I., 1956: *Heat balance of the Earth's surface*. U.S. Dept. of Commerce, Weather Bureau.

Budyko, M. I., and O. A. Drozdov, 1953: Characteristics of the moisture circulation in the atmosphere. **4**, 5–14.

Burde, G. I., and A. Zangvil, 2001: The estimation of regional precipitation recycling. part i: Review of recycling models. *Journal of Climate*, **14 (12)**, 2497–2508, https://doi.org/10.1175/1520-0442(2001)014<2497:TEORPR>2.0.CO;2, URL https://journals.ametsoc.org/jcli/article/14/12/2497/29526/The-Estimation-of-Regional-Precipitation-Recycling.

Cronin, T. W., K. A. Emanuel, and P. Molnar, 2015: Island precipitation enhancement and the diurnal cycle in radiative-convective equilibrium. *Quarterly Journal of the Royal Meteorological Society*, **141 (689)**, 1017–1034, https://doi.org/10.1002/qj.2443, URL https://rmets.onlinelibrary.wiley.com/doi/abs/10.1002/qj.2443.

Datseris, G., 2018: Dynamicalsystems.jl: A julia software library for chaos and nonlinear dynamics. *Journal of Open Source Software*, **3**, 598, https://doi.org/10.21105/joss.00598.

Datseris, G., and U. Parlitz, 2022: *Nonlinear Dynamics*. 2192-4791, Springer International Publishing, URL https://link.springer.com/book/9783030910334.

Eltahir, E. a. B., and R. L. Bras, 1994: Precipitation recycling in the amazon basin. *Quarterly Journal of the Royal Meteorological Society*, **120**, 861–880, https://doi.org/10.1002/qj.49712051806, URL https://onlinelibrary.wiley.com/doi/abs/10.1002/qj.49712051806.

Ent, R. J. v. d., H. H. G. Savenije, B. Schaefli, and S. C. Steele-Dunne, 2010: Origin and fate of atmospheric moisture over continents. *Water Resources Research*, **(9)**, https://doi.org/10.1029/2010WR009127, URL https://agupubs.onlinelibrary.wiley.com/doi/abs/10.1029/2010WR009127.

Entekhabi, D., 1994: A simple model of the hydrologic cycle and climate: 1. model construct and sensitivity to the land surface boundary. *Advances in Water Resources*, **17 (1)**, 79–91, https://doi.org/10.1016/0309-1708(94)90025-6, URL https://www.sciencedirect.com/science/article/pii/0309170894900256.

Entekhabi, D., and K. L. Brubaker, 1995: An analytic approach to modeling land-atmosphere interaction: 2. stochastic formulation. *Water Resources Research*, **31 (3)**, 633–643, https://doi.org/10.1029/94WR01773, URL https://onlinelibrary.wiley.com/doi/abs/10.1029/94WR01773.

Entekhabi, D., I. Rodriguez-Iturbe, and R. L. Bras, 1992: Variability in large-scale water balance with land surface-atmosphere interaction. *Journal of Climate*, **5**, 798–813, https://doi.org/10.1175/1520-0442(1992)005<0798:VILSWB>2.0.CO;2, URL https://journals.ametsoc.org/jcli/article/5/8/798/35919/Variability-in-Large-Scale-Water-Balance-with-Land.

Fiedler, S., and Coauthors, 2020: Simulated tropical precipitation assessed across three major phases of the coupled model intercomparison project (CMIP). *Monthly Weather Review*, **148 (9)**, 3653–3680, https://doi.org/10.1175/MWR-D-19-0404.1.

Hagemann, S., and T. Stacke, 2015: Impact of the soil hydrology scheme on simulated soil moisture memory. *Climate Dyn.*, **44**, 1731–1750, https://doi.org/10.1007/s00382-014-2221-6.

Hohenegger, C., and B. Stevens, 2022: Tropical continents rainier than expected from geometrical constraints.

Horton, R. e., 1943: Hydrologic interrelations between lands and oceans. *Eos, Transactions American Geophysical Union*, **24 (2)**, 753–764, https://doi.org/10.1029/TR024i002p00753, URL https://onlinelibrary.wiley.com/doi/abs/10.1029/TR024i002p00753.

Kumar, B. P., M. F. Cronin, S. Joseph, M. Ravichandran, and N. Sureshkumar, 2017: Latent heat flux sensitivity to sea surface temperature: Regional perspectives. *Journal of Climate*, **30 (1)**, 129–143, https://doi.org/10.1175/JCLI-D-16-0285.1, URL https://journals.ametsoc.org/view/journals/clim/30/1/jcli-d-16-0285.1.xml.

Lintner, B. R., P. Gentine, K. L. Findell, F. D'Andrea, A. H. Sobel, and G. D. Salvucci, 2013: An idealized prototype for large-scale land–atmosphere coupling. *Journal of Climate*, **26 (7)**, 2379–2389, https://doi.org/10.1175/JCLI-D-11-00561.1, URL https://journals.ametsoc.org/view/journals/clim/26/7/jcli-d-11-00561.1.xml.

Masunaga, H., and B. E. Mapes, 2020: A mechanism for the maintenance of sharp tropical margins. *Journal of the Atmospheric Sciences*, **77 (4)**, 1181–1197, https://doi.org/10.1175/JAS-D-19-0154.1, URL https://journals.ametsoc.org/view/journals/atsc/77/4/jas-d-19-0154.1.xml.

Ogino, S.-Y., M. D. Yamanaka, S. Mori, and J. Matsumoto, 2016: How much is the precipitation amount over the tropical coastal region? *Journal of Climate*, **29 (3)**, 1231–1236,

https://doi.org/10.1175/JCLI-D-15-0484.1, URL https://journals.ametsoc.org/view/journals/clim/29/3/jcli-d-15-0484.1.xml.

Ogino, S.-Y., M. D. Yamanaka, S. Mori, and J. Matsumoto, 2017: Tropical coastal dehydrator in global atmospheric water circulation. *Geophysical Research Letters*, **44 (22)**, 11,636–11,643, https://doi.org/https://doi.org/10.1002/2017GL075760, URL https://agupubs.onlinelibrary.wiley.com/doi/abs/10.1002/2017GL075760%4010.1002/%28ISSN%291944-8007.GRLHIGHLIGHTS2017.

Peixóto, J. P., and A. H. Oort, 1983: The atmospheric branch of the hydrological cycle and climate. *Variations in the Global Water Budget*, Springer Netherlands, 5–65, https://doi.org/10.1007/978-94-009-6954-4_2, URL https://doi.org/10.1007/978-94-009-6954-4_2.

Qian, J.-H., 2008: Why precipitation is mostly concentrated over islands in the maritime continent. *Journal of the Atmospheric Sciences*, **65 (4)**, 1428–1441, https://doi.org/10.1175/2007JAS2422.1, URL https://journals.ametsoc.org/jas/article/65/4/1428/26793/Why-Precipitation-Is-Mostly-Concentrated-over.

Rodriguez-Iturbe, I., D. Entekhabi, and R. L. Bras, 1991: Nonlinear dynamics of soil moisture at climate scales: 1. stochastic analysis. *Water Resources Research*, **27**, 1899–1906, https://doi.org/10.1029/91WR01035.

Schiro, K. A., J. D. Neelin, D. K. Adams, and B. R. Lintner, 2016: Deep convection and column water vapor over tropical land versus tropical ocean: A comparison between the amazon and the tropical western pacific. *Journal of the Atmospheric Sciences*, **73 (10)**, 4043–4063, https://doi.org/10.1175/JAS-D-16-0119.1, URL https://journals.ametsoc.org/view/journals/atsc/73/10/jas-d-16-0119.1.xml.

Schiro, K. A., S. C. Sullivan, Y.-H. Kuo, H. Su, P. Gentine, G. S. Elsaesser, J. H. Jiang, and J. D. Neelin, 2020: Environmental controls on tropical mesoscale convective system precipitation intensity. *Journal of the Atmospheric Sciences*, **77 (12)**, 4233–4249, https://doi.org/10.1175/JAS-D-20-0111.1, URL https://journals.ametsoc.org/view/journals/atsc/77/12/jas-d-20-0111.1.xml.

751 Seneviratne, S. I., T. Corti, E. L. Davin, M. Hirschi, E. B. Jaeger, I. Lehner, B. Orlowsky, and A. J.
752 Teuling, 2010: Investigating soil moisture–climate interactions in a changing climate: A review.
753 *Earth-Science Reviews*, **99 (3)**, 125–161, https://doi.org/10.1016/j.earscirev.2010.02.004, URL
754 https://www.sciencedirect.com/science/article/pii/S0012825210000139.

755 Shannon, C. E., 1948: A mathematical theory of communication. *The Bell System Technical*
756 *Journal*, **27 (3)**, 379–423, https://doi.org/10.1002/j.1538-7305.1948.tb01338.x.

757 Sobel, A. H., and G. Bellon, 2009: The effect of imposed drying on parameterized deep convection.
758 *Journal of the Atmospheric Sciences*, **66 (7)**, 2085–2096, https://doi.org/10.1175/2008JAS2926.
759 1, URL https://journals.ametsoc.org/view/journals/atsc/66/7/2008jas2926.1.xml.

760 Sobel, A. H., C. D. Burleyson, and S. E. Yuter, 2011: Rain on small tropical islands. *Journal of*
761 *Geophysical Research: Atmospheres*, **116**, https://doi.org/10.1029/2010JD014695, URL https:
762 //agupubs.onlinelibrary.wiley.com/doi/abs/10.1029/2010JD014695.

763 Ulrich, M., and G. Bellon, 2019: Superenhancement of precipitation at the center of tropical islands.
764 *Geophysical Research Letters*, **46 (24)**, 14 872–14 880, https://doi.org/10.1029/2019GL084947,
765 URL https://agupubs.onlinelibrary.wiley.com/doi/abs/10.1029/2019GL084947.

766 Wang, S., and A. H. Sobel, 2017: Factors controlling rain on small tropical islands: Diurnal cycle,
767 large-scale wind speed, and topography. *Journal of the Atmospheric Sciences*, **74 (11)**, 3515–
768 3532, https://doi.org/10.1175/JAS-D-16-0344.1, URL https://journals.ametsoc.org/jas/article/
769 74/11/3515/42168/Factors-Controlling-Rain-on-Small-Tropical-Islands.

770 Zhang, G. J., and M. J. McPhaden, 1995: The relationship between sea surface temperature and
771 latent heat flux in the equatorial pacific. *Journal of Climate*, **8 (3)**, 589–605, https://doi.org/10.
772 1175/1520-0442(1995)008<0589:TRBSST>2.0.CO;2, URL https://journals.ametsoc.org/view/
773 journals/clim/8/3/1520-0442_1995_008_0589_trbsst_2_0_co_2.xml.